Plant Physiology, January 2000, Vol. 122, pp. 243–254, www.plantphysiol.org © 2000 American Society of Plant Physiologists

The Delivery of Salts to the Xylem. Three Types of Anion Conductance in the Plasmalemma of the Xylem Parenchyma of Roots of Barley[1]

Barbara Köhler[2] and Klaus Raschke*

Albrecht-von-Haller-Institut für Pflanzenwissenschaften, Universität Göttingen, Untere Karspüle 2, 37073 Göttingen, Germany

To explore possible pathways for anions to enter the xylem in the root during the transport of salts to the shoot, we used the patch-clamp method on protoplasts prepared from the xylem parenchyma of barley (*Hordeum vulgare* L.) plants. K^+ currents were suppressed by tetraethylammonium or *N*-methylglucamine in the solutions in the pipette and the bath, and the permeating anions were Cl^- or NO_3^-. We recorded the activities of three distinct anion conductances: (a) an inwardly rectifying anion channel (X-IRAC), characterized by activation at hyperpolarization and open times of up to several seconds; (b) a quickly activating anion conductance (X-QUAC), important for anion efflux at voltages between −50 mV and the equilibrium potential of the prevailing anion; and (c) a slowly activating anion conductance (X-SLAC), activating above −100 mV. Both X-IRAC and X-QUAC were permeable for Cl^- and NO_3^-; X-QUAC was also permeable for malate. The occurrence of X-IRAC became more frequent with an increase in cytoplasmic Ca^{2+}, while the occurrence of X-QUAC decreased. Anion currents through X-SLAC, and particularly through X-QUAC, were estimated to be large enough to account for reported rates of xylem loading, which is in accordance with the notion that xylem loading is a passive process.

Three pathways are thought to exist for the radial transport of inorganic nutrients from the root cortex into the stele: the apoplastic, the symplastic, and the transcellular routes (Pitman, 1982; Clarkson, 1993). However, the hydrophobic Casparian strip in the walls of the endodermis blocks the apoplastic path for salts (Caspary, 1865–1866; Marschner, 1995), and, therefore, ions can enter the stele only by passing plasma membranes at least twice to reach the transport system from the root to the shoot, once upon entry into the symplast of the root and again during their release into the apoplast of the stele. It is this discharge that was the subject of the present study. How it takes place was a matter of speculation for decades (for instance, see Marschner, 1995). Knowledge of the transport mechanisms involved in xylem loading and their control would contribute to our understanding of a controlled nutrient transfer from the root to the shoot.

Results of patch-clamp experiments with isolated protoplasts prepared from barley (*Hordeum vulgare* L.) roots showed that salt efflux from cells of the xylem parenchyma can occur passively through ion channels (Wegner and Raschke, 1994). The activity of an outward rectifier for K^+ would allow cations to pass into the apoplast of the stele (Wegner and Raschke, 1994; Wegner and De Boer, 1997). A similar type of channel was found in roots of maize (Roberts and Tester, 1995). Recently, the amino acid sequence of a K^+-specific outwardly rectifying channel from Arabidopsis was reported; this protein was expressed exclusively in the root stele (Gaymard et al., 1998). Salt loading is an electroneutral process. It requires the presence of anion conductances that match the cation permeabilities. Little information on such transport proteins is available to date for the xylem parenchyma. Wegner and Raschke (1994) described an anion channel in cells from this tissue; however, its transport capacity seemed insufficient to account for anion loading. We therefore continued the exploration of anion conductances, again using protoplasts prepared from the xylem parenchyma of barley roots. We discovered activities for three types of anion conductances exhibiting different characteristics, and evaluated their importance for the release of salts into the xylem.

MATERIALS AND METHODS

Plant Cultivation and Protoplast Isolation

Barley (*Hordeum vulgare* L. cv Apex; F. von Lochow-Petkus, Bergen, Germany) was grown in a hydroponic growth facility on aerated full-strength Long-Ashton NO_3^--type solution (Hewitt and Smith, 1975) that was changed weekly. Plants were grown at 20°C from 4 to 22 h and at 18°C from 22 to 4 h. They were illuminated at 300 μmol m^{-2} s^{-1} from fluorescent tubes (L65W/25S, Osram, Munich, Germany) from 8 to 20 h. Xylem parenchyma protoplasts were isolated from roots of 3- to 5-week-old plants as described by Wegner and Raschke (1994). Nodal roots 4 to 6 cm long without lateral root formation were selected, and the apical 1 to 2 cm cut off. The stele was pulled out of the cortex, and the distal 1 to 2 cm of the stele was chopped into millimeter segments and incubated in enzyme solution for 2.5 h at 20°C (2% [w/v] cellulase

[1] This work was supported by grants from the Deutsche Forschungsgemeinschaft to K.R.

[2] Present address: Laboratory of Plant Physiology and Biophysics, University of London, Wye College, Wye, Kent TN25 5AH, UK; e-mail sbs99bk@wye.ac.uk.

* Corresponding author; e-mail kraschk@gwdg.de; fax 49–551–397823.

Onozuka R10, Yakult Honsha, Tokyo; 0.02% [w/v] pectolyase Y-23, Seishin Pharmaceutical, Tokyo; 2% [w/v] bovine serum albumin, 10 mM Na ascorbate, and 1 mM $CaCl_2$; pH 5.5; 500 mosmol kg^{-1}). The enzyme was filtered in three steps (200-, 100-, and 20-μm mesh) using 500 mM sorbitol augmented with 1 mM $CaCl_2$ as washing medium. Protoplasts were then isolated by two centrifugation steps (120*g* for 10 min each).

Electrical Recording and Solutions

Anion currents were investigated with the patch-clamp technique (Hamill et al., 1981) using an amplifier (EPC-7, List Electronic, Darmstadt, Germany) and a personal computer (Mega ST4, Atari, Sunnyvale, CA) with the E9-screen program (HEKA Elektronik, Lambrecht, Germany) for pulse generation. Capacitive currents were measured and corrected for with the amplifier. Access resistances (between 5.6 and 20 MΩ) were measured with the amplifier and corrected for using the method of Marty and Neher (1995) when current-voltage curves were plotted.

Data were low-pass filtered at the frequencies given in the figure legends with an eight-pole Bessel filter (−3 dB corner frequency; Frequency Devices, Haverhill, MA) and stored on the computer's hard drive or on videotape (Panasonic NV–H75, Matsushita Electric Industrial, Osaka) via an ITC 16 interface (Instrutech, Elmont, NY) or a VR–10 interface (Instrutech), respectively. For data transfer from videotape to hard disk, the program Acquire (H. Affolter and F. Sigworth, Instrutech) was used. The sample frequency was at least four times the filter frequency.

Pipettes were pulled (L/M–3P–A, List Electronic, Darmstadt, Germany) from borosilicate glass capillaries (Kimax–51, Kimble Products, Vineland, NY), insulated with Sylgard (Dow Corning, Midland, MI), and fire-polished (L/M–CPZ–101, List Electronic). Tip resistances were 5 to 20 MΩ. Electrode tip potentials were nulled during the patch-clamp procedure. All recordings were made at temperatures between 22°C and 24°C. The reference electrode was fixed in a tube filled with 200 mM KCl (agar bridge) or with the external solution.

Solutions were designed for the detection of anion currents. K^+ currents were suppressed by tetraethylammonium (TEA^+) or *N*-methylglucamine (NMG^+). The standard extracellular solution contained: 30 mM TEA-Cl (or NMG-Cl), 5 mM $Ca(Glc)_2$, 2 mM $MgCl_2$, and 10 mM 2-(N-morpholino)-ethanesulfonic acid (MES), and was adjusted to pH 5.8 with Tris. The osmolality was adjusted to 500 mosmol kg^{-1} with mannitol. Two intracellular solutions were used: the low-Ca^{2+} solution contained 120 mM TEA-Cl (or NMG-Cl), 0.15 μM free Ca^{2+} as 4.3 mM $Ca(Glc)_2$, 10 mM EGTA, 2 mM MgATP, 2 mM $MgCl_2$, and 10 mM Tris, and was adjusted to pH 7.2 with MES; the high Ca^{2+}solution was the same as the low Ca^{2+}, except with 5 μM free Ca^{2+} as 4.5 mM $Ca(Glc)_2$ and 10 mM *N*-hydroxyethyl-EDTA in place of 10 mM EGTA. In each case, osmolality was adjusted to 530 mosmol kg^{-1} with mannitol. This was verified by a water-vapor pressure osmometer (5100 C, Wescor, Logan, UT). Total and free concentrations of divalent cations were computed using the program Calcium (Führ et al., 1993). Variations of the solutions are indicated in the figure legends. All solutions were filtered with a 0.22-μm filter before use and stored at −20°C.

Data Analysis

Data were analyzed with the software packages Review (Instrutech), Tac (Instrutech), and SigmaPlot (Jandel, San Rafael, CA). Liquid junction potentials between pipette and bath solutions have been measured and all membrane voltages were corrected for according to the method of Neher (1992). Correction was done if the magnitudes of the liquid junction potentials were larger than 3 mV. This was the case when 30 mM TEA-Cl (−7 mV) or 30 mM NMG-Cl (−8 mV) was in the bath. Liquid junction potentials were the same with low- or high-Ca^{2+} solutions in the pipette. In the tests for ion selectivity, starting with TEA-NO_3 or $(TEA)_2$-malate, −7 or −8 mV were subtracted, respectively. Ion activities were calculated when ionic equilibrium potentials were critical for data interpretation. Means of measured data are given with SD.

For single-channel analysis, current versus voltage curves were constructed from single-channel amplitudes determined by measuring the amplitudes in continuous recordings and fitting the resulting histograms with Gaussian functions, or by calculation of the mean single-channel current according to:

$$\frac{\sum (\text{Dwell time} \cdot \text{Current})}{\sum (\text{Dwell time} \cdot \text{Level number})} \quad (1)$$

Fast-voltage ramps were applied for the recording of the current through an open channel. For correction of the background current, the current flowing when the channel was closed was subtracted (see Tyerman and Findlay, 1989).

The mean open time was calculated according to:

$$\frac{\sum (\text{Dwell time} \cdot \text{Level number})}{\text{Number of openings}} \quad (2)$$

Since there was more than one channel active in the experiments, the channel activity, or the number of channels (n) times the open probability (P) was calculated:

$$nP = \frac{\sum (\text{Dwell time} \cdot \text{Level number})}{\text{Total time}} \quad (3)$$

The current at the baseline was measured to ensure that all channels were closed. If this was not the case, the nP value was corrected.

Current-voltage curves derived from whole-cell recordings were constructed from a series of voltage steps, which are given in the figures. Usually the current 10 ms into a voltage step (the "instantaneous current") and the current at the end of a voltage step (after a new steady state had been established) were plotted against the voltage. Between voltage steps, voltage was clamped at the holding potential for the current to settle.

Protoplasts varied in size. Their capacities were between 8 and 23 pF. Note that each parenchyma cell disintegrated

into an average of six protoplasts during preparation (Wegner and Raschke, 1994). To compare measurements on different cells, channel activities and currents were related to the membrane area. The specific capacity of xylem parenchyma protoplast was 0.9 μF cm^{-2} (Wegner and Raschke, 1994).

Permeability ratios were determined under bi-ionic conditions. The intracellular solution contained 120 mM TEA-Cl and the extracellular solution contained 30 mM TEA-NO_3 or $(TEA)_2$-malate, respectively. After determination of the reversal potential, permeability ratios were calculated by the Goldman-Hodgkin-Katz-voltage equation (Hille, 1992):

$$\frac{P_m}{P_n} = \frac{z_n^2}{z_m^2} \cdot \frac{\exp(z_m E_{rev} F/RT) - 1}{\exp(z_n E_{rev} F/RT) - 1} \cdot \frac{a_{ni} \cdot \exp(z_n E_{rev} F/RT) - a_{no}}{a_{mo} - a_{mi} \cdot \exp(z_m E_{rev} F/RT)} \quad (4)$$

where P is the permeability, z is the valence, E_{rev} is the reversal potential, F is Faraday's constant, R is the gas constant, T is the absolute temperature, a is the activity, m and n are the ion species, and o and i are the extracellular and intracellular sides. This equation was derived from the condition that at the reversal potential the sum of the ion currents is zero:

$$I = F \sum_v z_v \phi_v = F(z_n \cdot \phi_n + z_m \cdot \phi_m) = 0 \quad (5)$$

where I is the ion flux density, z_ν is the valence of the ion species ν, and ϕ_ν is the flux density of ion species ν. Ion flux densities (ϕ) were estimated by applying the Nernst-Planck equation (Adam et al., 1988):

$$\phi_v = P_v z_v \frac{FE}{RT} \frac{a_{vi} \cdot \exp(z_v FE/RT) - a_{vo}}{\exp(z_v FE/RT) - 1} \quad (6)$$

where P_ν is the permeability coefficient for ion species ν, and E is the membrane voltage. Substitution of Equation 6 (for $\nu = m$ and for $\nu = n$) into Equation 5, followed by rearrangement, led to Equation 4.

Sign Convention and Estimation of Ion Fluxes from Xylem Parenchyma into the Apoplast

Membrane potentials are defined as the voltage on the cytoplasmic side of the membrane with respect to the physiological outside. In the "whole-cell"—and in the "outside-out"—configuration, the inner side of the membrane is turned toward the pipette. Thus, the voltage between the pipette and the reference electrode corresponds to the membrane potential. A negative current corresponds to an anion efflux from the protoplast and to a K^+ influx into the protoplast.

To evaluate the putative role of anion conductances in xylem loading, ionic fluxes were calculated from electrophysiological data. Since salt export is an electroneutral process, anion efflux must equal cation efflux. Based on the assumptions that ion efflux occurred through K^+-selective outwardly rectifying channels (KORC) (data from Wegner and De Boer, 1997) and through one of the anion conductances each time, and that the membrane potential is a pure diffusion potential, a hypothetical membrane potential at which salt efflux would be possible was determined. Ion fluxes from cytoplasm into the xylem vessels (J_{CX}) were calculated from current densities (j) at this hypothetical membrane:

$$J_{CX} = \frac{j \cdot A}{z \cdot F \cdot b} \quad (7)$$

Where A is the cell surface, b is the fresh weight, z is the valence, and F is Faraday's constant. All xylem parenchyma cells from the differentiated metaxylem likely participate in xylem loading (see Fig. 1 in Wegner and Raschke, 1994). Therefore, the current density was multiplied with the cell surface to obtain ion fluxes, which then were related to fresh weight. Values of cell surface (0.42 cm^2 cm^{-1} root length) and fresh weight (3.9 mg cm^{-1} root length) were provided by L.H. Wegner (personal communication). Whole-cell currents through inwardly rectifying anion channels (X-IRAC) were determined by multiplying the single-channel current by the channel activity (nP).

RESULTS

Because we wished to discover anion conductances, we suppressed K^+ currents by the use of TEA^+ or NMG^+ in the place of K^+ in the solutions of our patch-clamp experiments. Considering that usually Ca^{2+} is required to activate anion channels (Hedrich et al., 1990; Tester, 1990), we began our experimentation with 5 μM Ca^{2+} in the pipette. Under these conditions, X-IRAC (X stands for xylem parenchyma) appeared as the predominant anion conductance. It was active in 34% of the examined protoplasts and was readily recognized in the whole-cell configuration by the appearance of single-channel events. During the experimental characterization of X-IRAC, we applied short hyperpolarizing and depolarizing voltage pulses and discovered rapidly activating and inactivating currents, which we interpreted as displays of the quickly activating anion con-

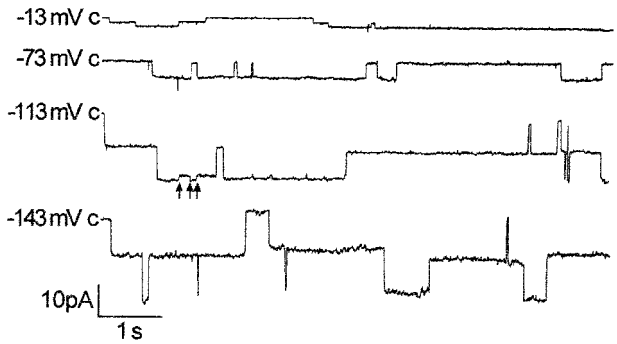

Figure 1. Example of single-channel recordings of X-IRAC in the whole-cell configuration (from one protoplast out of seven). The data were filtered at 100 Hz. In the pipette was high-Ca^{2+} solution; in the bath was the standard solution (see "Materials and Methods"). The letter "c" at the beginning of each trace indicates the current level at the closed state. Downward changes correspond to channel openings. Arrows point to changes in open-channel conductance levels (presumed subconductance states).

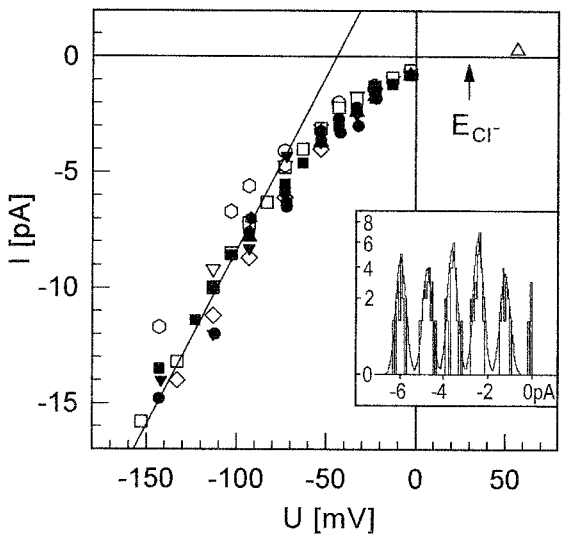

Figure 2. Current-voltage relationship of X-IRAC. Currents were derived from single-channel recordings on six different cells exposed to 0.15 μM Ca^{2+} in the pipette (white symbols, five of the upright triangles are hidden behind other symbols) and on six different cells exposed to 5 μM Ca^{2+} in the pipette (black symbols). A line was fitted to the means of currents at voltages between −159 and −93 mV; it did not pass through the origin ($r^2 = 0.89$), which would have been the case if rectification was the result of a concentration gradient, as described by the Goldman-Hodgkin-Katz current equation (Hille, 1992). Inset, Logarithm of the frequency of discrete current events as they appeared in recordings such as the one shown in Figure 1, plotted against current. This example was taken from a recording obtained at 13 mV. Such distributions were used to determine the number of simultaneously active channels in a protoplast (here it was 5). Distances between the means of Gaussian functions fitted to the data indicate magnitudes of single-channel currents. In the pipette was either the high- or low-Ca^{2+} solution; in the bath was the standard solution (see "Materials and Methods").

ductance (X-QUAC). This anion conductance could further be identified by a concavity in the current-voltage curve that was displayed when voltages were raised above −40 mV. The conductance X-QUAC also occurred when the Ca^{2+} concentration in the pipette was lowered to 0.15 μM. A third anion conductance appeared during long voltage pulses, which deactivated slowly. We called it the slowly activating anion conductance (X-SLAC), which occurred in 7% of the tested protoplasts. The current-voltage relationships of all three anion conductances had in common a change in sign at or close to the Nernst potential of the major anion in the solutions (Cl^- or NO_3^-).

X-IRAC

Single-channel events with slow gating characteristics became visible in the whole-cell configuration, and indicated low channel density or activity of X-IRAC (Fig. 1). This anion channel was active between −180 and 50 mV. Different levels of open-channel conductances appeared (Fig. 1), especially in the negative voltage range. In the experiments, some of which lasted as long as 40 min, no inactivation of X-IRAC occurred. The mean open time was in the range of seconds; for instance, at −73 mV, it was 1.2 ± 0.5 s ($n = 6$, 5 μM Ca^{2+} in the pipette). Current-voltage relationships were derived from single-channel recordings (Fig. 2). They showed that the sign of the current reversed near E_{Cl^-}. Using standard solutions, the Nernst potential of Cl^- was 30 mV, whereas the Nernst potentials of TEA^+ or NMG^+, and that of Ca^{2+} were located at −32 and 143 mV, respectively. Currents recorded during the application of voltage ramps while an X-IRAC channel stayed open were zero at 27 ± 4 mV ($n = 16$) (see also comparison of the currents with Cl^- and NO_3^- in the bath in Fig. 4). Gaussian functions were fitted to the single-channel current frequencies (the inset in Fig. 2 shows an example). They were spaced at equal current intervals, indicating that usually more than one channel was active in a protoplast; up to 14 simultaneously active channels could be distinguished in a single (sub) protoplast. Single-channel currents did not depend on internal Ca^{2+} concentrations (Fig. 2).

Currents increased with hyperpolarization, but remained small at positive potentials (Fig. 2). This inward rectification by X-IRAC was not caused by a concentration gradient (legend to Fig. 2). In standard solutions the chord conductance of X-IRAC decreased from 71 pS at −133 mV ($n = 2$) to 47 pS at −73 mV ($n = 5$) and further to 13 pS at −3 mV ($n = 3$).

If the Ca^{2+} concentration in the pipette was raised from 0.15 to 5 μM, the probability of appearance of X-IRAC increased. At 0.15 μM, X-IRAC was active in nine out of 84 protoplasts, corresponding to 11% of the examined protoplasts; and at 5 μM, activity appeared in 25 out of 74 protoplasts, corresponding to 34%. A χ^2 test showed that the association between increasing the concentration of Ca^{2+} and increasing activity of X-IRAC was significant at a level of $P = 0.005$ ($\chi^2 = 7.98 > 7.88$). The channel activity (nP) of X-IRAC fluctuated strongly (Fig. 3), varying be-

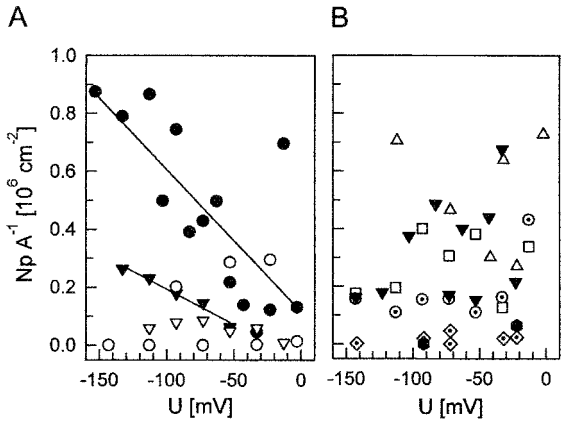

Figure 3. Channel activity (nP) per unit membrane area (A) of X-IRAC with low-Ca^{2+} solution (0.15μm) (A) and high-Ca^{2+} solution (5 μM) (B) in the pipette.; in the bath was the standard solution (see "Materials and Methods"). Results are from four (A) and six (B) protoplasts (identified by different symbols). Lines in A represent regressions of data from two individual protoplasts; in these two instances, channel activity declined with increasing voltage, with r^2 of 0.97 and 0.57, respectively.

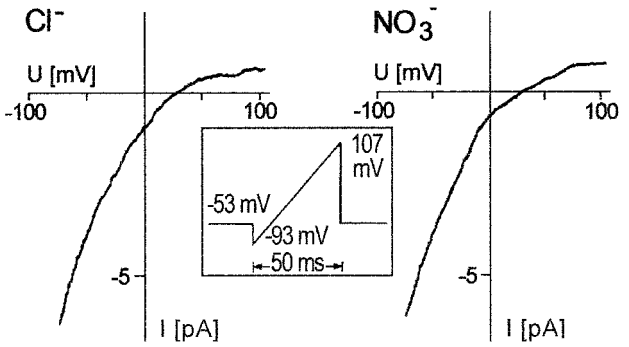

Figure 4. Current responses of X-IRAC to voltage ramps of 50-ms duration (inset), showing that replacement of external Cl^- by NO_3^- had no effect. Residual currents (flowing when all anion channels were closed) were subtracted. The current-voltage curve with external Cl^- is an average of eight ramps; that with external NO_3^- of 17 ramps. This experiment was conducted on one protoplast in the whole-cell configuration (replicated with four more protoplasts). The filter frequency was 100 Hz. In the pipette was low-Ca^{2+} solution; in the bath was the standard solution with the indicated changes in the major anion (see "Materials and Methods").

tween 0.05×10^6 cm^{-2} and 0.9×10^6 cm^{-2}. The mean value of *nP* over the whole voltage range was $0.26 \pm 0.27 \times 10^6$ cm^{-2} with 0.15 μM Ca^{2+} in the pipette ($n = 33$) and $0.25 \pm 0.21 \times 10^6$ cm^{-2} with 5 μM Ca^{2+} in the pipette ($n = 39$, calculated from the data shown in Fig. 3). Nevertheless, with 0.15 μM Ca^{2+} in the pipette, channel activity declined with increasing voltage in two out of the four protoplasts tested (Fig. 3A); however, in general, the intracellular Ca^{2+} concentration did not affect channel activity of X-IRAC significantly. Changes in the external Ca^{2+} concentration from 5 to 40 mM, or to 1 mM, did not influence the occurrence of X-IRAC or its current-voltage relationship (not shown).

X-IRAC was equally permeable for NO_3^- and Cl^-. Replacement of Cl^- by NO_3^- in the bath did not alter the current-voltage curves ($n = 5$); current responses and reversal potentials were nearly identical with either one of the anions present (Fig. 4); with external NO_3^- the reversal potential was 27 ± 2 mV ($n = 5$). Single-channel currents were determined at membrane potentials of −93, −23, and 97 mV, and were found to have been −7.6 ± 1 pA, −1.6 ± 0.1 pA and 0.6 ± 0.3 pA, respectively ($n = 5$). With external Cl^-, the corresponding single-channel currents were −7.5 ± 0.8 pA, −1.3 ± 0.6 pA, and 0.5 ± 0.3 pA ($n = 6$). External NO_3^- did not affect channel activity (*nP*), which was 0.3 ± 0.28 ($n = 28$, four protoplasts). In one case, *nP* decreased linearly with increasing potentials (not shown).

X-QUAC

Typical for this conductance was its rapid activation upon voltage jumps from a holding potential of −43 mV to both more positive and more negative values (Fig. 5). X-QUAC was active between −200 and 100 mV. In all experiments in which X-QUAC dominated cell conductance, the sign of the currents reversed at 25 ± 5 mV ($n = 20$), a value slightly more negative than the Nernst potential of Cl^-. Leak currents were not subtracted from the recorded values; they may have caused this shift, and they could have included the activity of an electrogenic pump (Köhler and Raschke, 1998b). The current-voltage curves exhibited a maximum near −40 mV, where the magnitude of the current was small, and a minimum near 0 mV. The

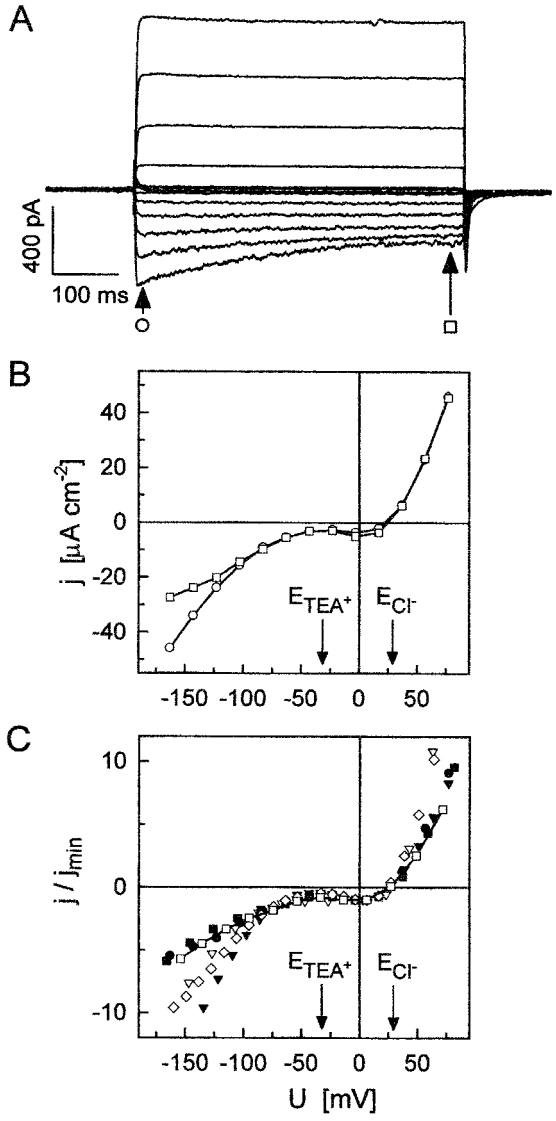

Figure 5. Activation and current-voltage relationship of X-QUAC. A, From a holding potential of −43 mV (for 10 s), pulses of 500-ms duration were applied in decrements of 20 mV, covering the voltage range between 77 and −163 mV; whole-cell configuration. The filter frequency was 1 kHz. In the pipette was low-Ca^{2+} solution; in the bath was the standard solution (see "Materials and Methods"). B, Current-voltage relationship of X-QUAC derived from the data shown in A. Current densities (j) measured 10 ms (○) and 500 ms (□) after initiation of a voltage step (arrows in A) were plotted against voltage. C, Currents measured on six protoplasts (identified by different symbols) at the end of 500 ms-pulses plotted against voltage. Relationships were normalized with respect to the current minimum, j_{min}, appearing at a membrane voltage near 0 mV. Data from the experiment shown in A and B are included (□) and joined by a line.

magnitude of the currents through X-QUAC varied among protoplasts; the current density at the minimum was 2.2 ± 2 μA cm^{-2} (n = 20). To bring out common current-voltage characteristics of X-QUAC, currents of six protoplasts were normalized with respect to their minimum at 0 mV and shown in Figure 5C. At hyperpolarization, X-QUAC inactivated partially (Fig. 5A). Tail current experiments were performed after partial and complete inactivation of the inward current. Currents reversed between 27 and 37 mV, near the Nernst potential of Cl^- (n = 6); they were carried by Cl^- (Fig. 6). The same conclusion applied to the outward currents (n = 6, not shown, but confirmed by pulse experiments such as the one presented in Fig. 5).

A low concentration of Ca^{2+} in the "cytoplasm" enhanced the activity of X-QUAC, in contrast to the Ca^{2+} dependence of the activity of X-IRAC: With 5 μM Ca^{2+} in the pipette, X-QUAC appeared in seven out of 68 protoplasts, corresponding to 10% of the examined protoplasts; with 0.15 μM Ca^{2+}, X-QUAC activity was seen in 16 out of 59 protoplasts, corresponding to 27% of the examined protoplasts. A χ^2 test resulted in a value of 4.16, which indicated that the association between increasing Ca^{2+} concentration in the "cytoplasm" and decreasing activity of X-QUAC was significant at a level of P = 0.05 ($\chi^2 > 3.84$). Changes in the extracellular Ca^{2+} concentration between 1 and 40 mM did not affect the occurrence of X-QUAC nor its current-voltage relationship (not shown).

The conductance X-QUAC was permeable not only for Cl^-, but also for NO_3^- and malate^{2-} (Fig. 7). In the presence of external NO_3^- (30 mM), the reversal potential was near 9 mV; it shifted to 55 mV after replacement by 30 mM malate (Table I). From the reversal potentials, relative permeabilities (with respect to that for Cl^-) were calculated (Table I). For $P_{NO_3^-}/P_{Cl^-}$, the ratio was 3. Because, at pH 5.8 in the external solution, 83% of the malate was charged 2-fold (pK_1 = 3.5; pK_2 = 5.1), we assumed that malate^{2-} permeated the membrane, and we estimated $P_{malate^{2-}}/P_{Cl^-}$ to have been about 0.28 (for single-charged malate, the permeability ratio would have been about 48; Table I). Most of these experiments were done on different protoplasts.

To facilitate comparisons, current-voltage curves were normalized with respect to the current minimum that in each case appeared in the voltage range between −50 mV and the particular reversal potentials; Figure 7B). (This voltage range is probably the most important one for salt release into the xylem; see "Discussion"). The position of the minimum depended on the species of the external anion. With external NO_3^-, it was about 20 mV more negative than with external Cl^-, and with external malate, it was about 15 mV more positive than with external Cl^-. Considering the absolute magnitudes of the anion effluxes in the mentioned voltage range (Fig. 7A), we recognize that replacement of external NO_3^- by malate led to a reduction of anion loss, although the electromotive force acting on the anion in the cell was larger with malate than with NO_3^-. This result was obtained on one and the same protoplast; it could not have been accidental, despite the generally wide variation among cells in the magnitude of their anion currents. We do not know yet whether the disparity between malate currents that appeared at negative membrane voltages (Fig. 7B) points to variations in a hypothetical binding site for malate.

X-SLAC

This conductance appeared in seven out of 104 experiments when the internal Ca^{2+} concentration was kept relatively low (at 0.15 μM), and activated at potentials higher than −100 mV. In the experiment shown in Figure 8, it was activated at a holding potential of 37 mV. Polarizing pulses resulted in gradual deactivations, illustrating the slow gating behavior of X-SLAC. The increase in current following the step from 37 to 67 mV made it clear that at 37 mV, X-SLAC was not yet fully activated (Fig. 8A). The reversal potential of about 30 mV affirms a selectivity of X-SLAC for the anion Cl^-, and the current densities of both the instantaneous current (measured 10 ms after the voltage step, white symbols in Fig. 8B) and the steady-state current (as extrapolated from exponential functions fitted to the deactivation records, black symbols in Fig. 8B), reversed near

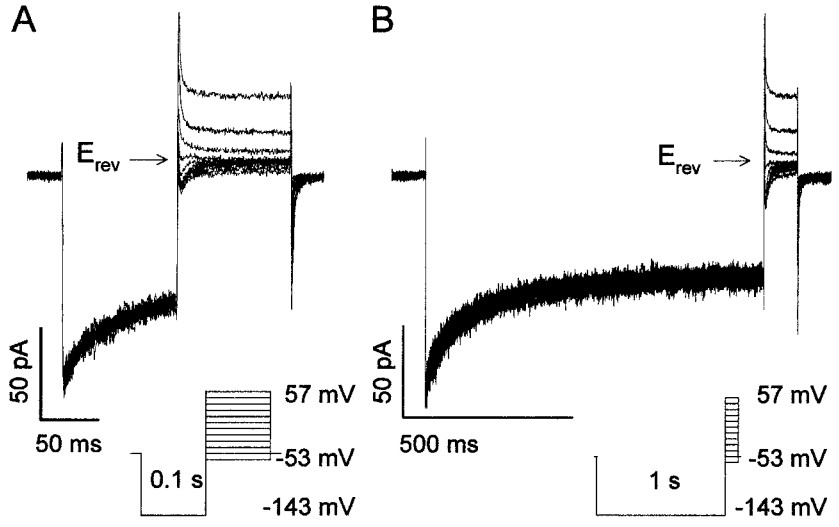

Figure 6. X-QUAC, tail-current experiments. After clamping the voltage at −143 mV for 100 ms (A) or 1 s (B), voltage pulses with a duration of 100 ms were applied between 57 and −53 mV (insets). E_{rev}, The currents reversed between 17 and 27 mV (A) or between 27 and 37 mV (B). Whole-cell configuration, filter frequency was 1 kHz. In the pipette was low-Ca^{2+} solution; in the bath was the standard solution (see "Materials and Methods").

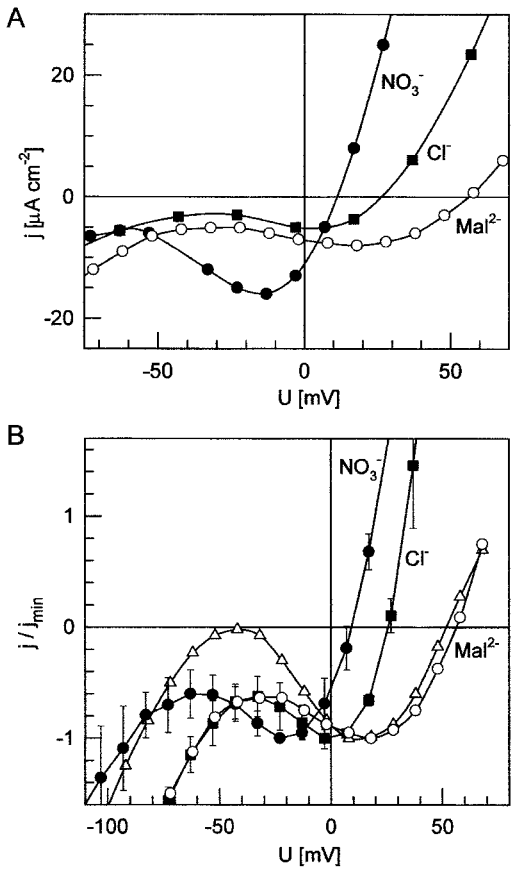

Figure 7. A, Current-voltage relationships of X-QUAC for three different anions in the external solution, Cl^- (■), NO_3^- (●), and $malate^{2-}$ (○). The data shown for NO_3^- and $malate^{2-}$ were obtained on one protoplast after replacing external TEA-NO_3 with $(TEA)_2$-malate. B, Currents were normalized with respect to their minima that appeared at membrane voltages between −50 mV and the reversal potentials, average currents of Cl^- (n = 5) and NO_3^- (n = 4), and two individual examples for currents of $malate^{2-}$ (white symbols). A and B, Lines extending to the borders of the diagrams indicate that some data points were outside the ranges of the panels. Experimental procedure similar to that shown in Figure 5. In the pipette was low-Ca^{2+} solution; in the bath was the standard solution with the indicated changes in the major anion (see "Materials and Methods").

Table I. *X-QUAC is permeable for NO_3^- and malate*

Permeability ratios with respect to Cl^- were calculated from reversal potentials as described in "Material and Methods." For the determination of reversal potentials, anions were varied in the bath. The low-Ca^{2+} solution was used in the pipette. P_x, Permeability for NO_3^- (n = 4) or malate (n = 2). In the case of malate, permeability ratios were calculated for both the double- and the single-charged form.

Anion (x) in the Bath	Reversal Potential	P_x/P_{Cl^-}
	mV	
NO_3^- (30 mM)	8, 8, 11, 12	3.4, 3.4, 3.0, 2.8
Malate (30 mM)		
As $malate^{2-}$ (25 mM)	52, 57	0.32, 0.24
As $malate^-$ (5 mM)	52, 57	55, 42

the equilibrium potential of Cl^-. (The instantaneous current represents the current through channels that were activated during the time at the conditioning voltage of 37 mV).

The steady-state current-voltage curve proves that X-SLAC stays active at membrane voltages greater than −100 mV (more positive than −100 mV). Clamping the voltage at hyperpolarized values led to a closure of X-SLAC; this is demonstrated in Figure 9. After a holding voltage of −123 mV, voltage steps elicited only insignificant current changes during the 500 ms-pulses (Fig. 9B), in contrast to steps starting from a holding potential of 37 mV (Fig. 9A). The activation of X-SLAC appearing during long pulses was very slow; after a change from −123 mV to 67 mV, only a small fraction of the steady-state conductance had just come into view after 5 s (not shown). The ensuing small increase in current caused a shift of the reversal voltage to positive values (n = 2, not shown).

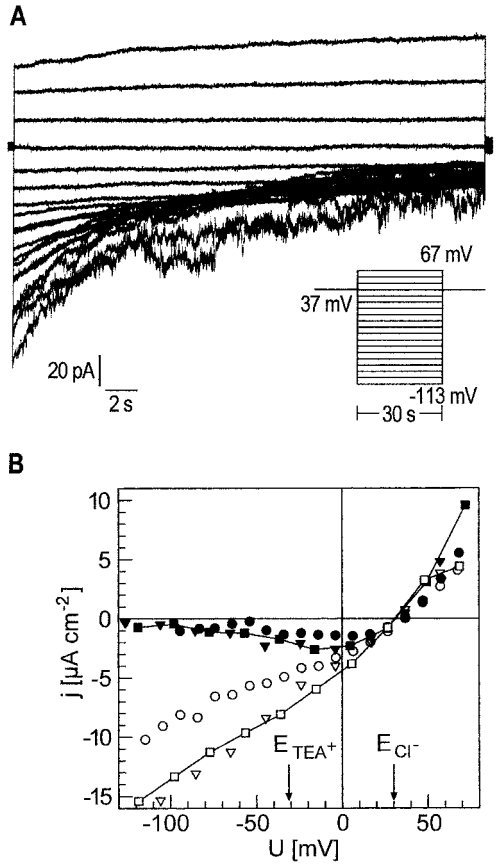

Figure 8. A, Deactivation of X-SLAC recorded while running the voltage protocol shown in the inset; between pulses, the voltage was clamped to 37 mV for 60 s each. Filter frequency was 400 Hz. At negative potentials, currents were noisy occasionally. B, Current-voltage relationship of X-SLAC in three protoplasts. Current densities determined 10 ms after triggering a voltage pulse (white symbols) and after a new steady state had been established (black symbols) were plotted against the voltage. Squares indicate values derived from the records shown in A. Steady-state currents were determined by extrapolation of exponential functions fitted to the deactivation curves. Nernst potentials were 30 mV (Cl^-), −32 mV (TEA^+), and 143 mV (Ca^{2+}). In the pipette was low-Ca^{2+} solution; in the bath was the standard solution (see "Materials and Methods").

The gating characteristics of X-QUAC and X-SLAC were clearly distinct. Only minute time-dependent changes of current through X-SLAC occurred during pulses of 500 ms duration, in contrast to the pronounced changes of currents through X-QUAC.

Simultaneous Activity of X-QUAC and KORC

A condition sine qua non for the loading of salts into the xylem is the concurrent activity of anion and cation conductances. In solutions containing KCl, a slow activation of the KORC appeared superimposed on the traces of the quickly activated X-QUAC (Fig. 10A). After replacement of the external KCl with TEA-Cl, K^+ currents were inhibited and the currents through X-QUAC retained (Fig. 10B) their typical current-voltage characteristics (Fig. 10C). The reversal potential shifted to $E_{Cl}{}^-$. An activity of the inwardly rectifying K^+ channel (KIRC) was never observed simultaneously with that of X-QUAC, although KIRC appeared more often than KORC. The conductance KIRC was active in 14 out of 43 protoplasts, KORC only in three.

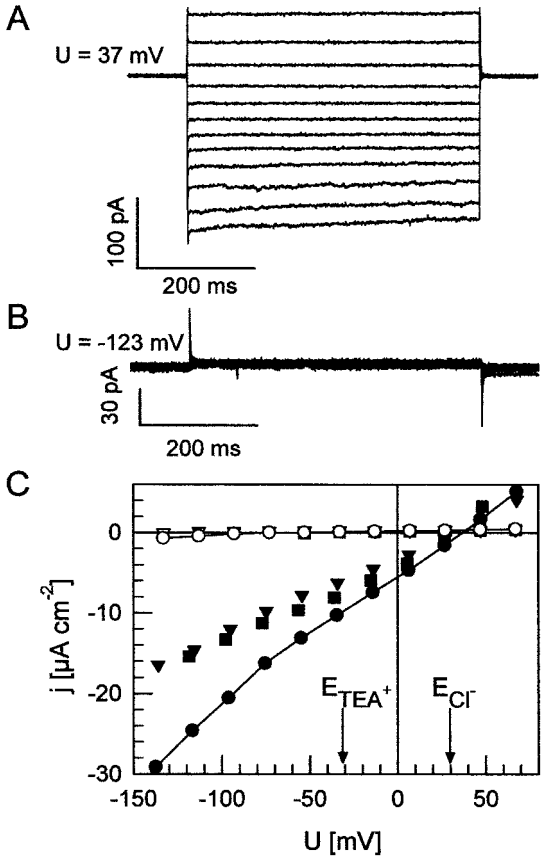

Figure 9. No activation of X-SLAC at hyperpolarization. After holding the protoplast for 60 s at conditioning voltages of 37 mV (A) or −123 mV (B), pulses of 500-ms duration were applied in 20-mV steps to voltages between 87 mV and −137 mV. C, Current-voltage relationships of three protoplasts determined 10 ms after a voltage change from a conditioning voltage of 37 mV (black symbols) or of −123 mV (white symbols). Circles joined by lines represent values derived from the experiment shown in A. Filter frequency was 400 Hz. In the pipette was low-Ca^{2+} solution; in the bath was the standard solution (see "Materials and Methods").

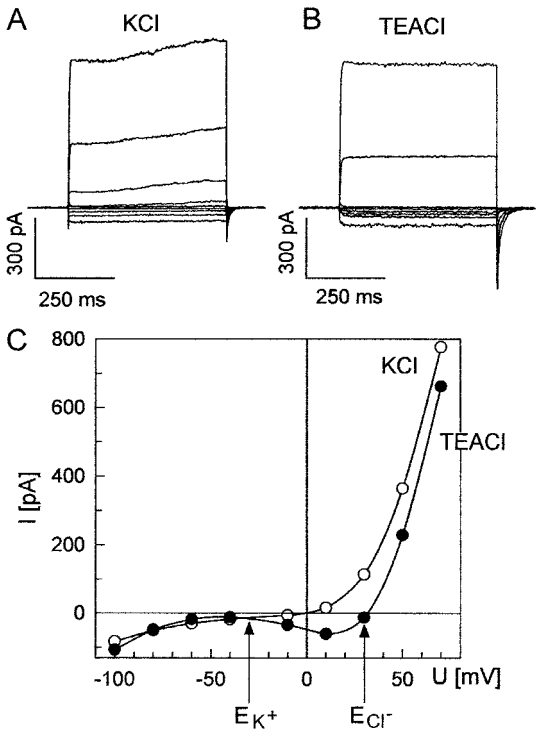

Figure 10. A, Simultaneous activity of X-QUAC and KORC. B, Inhibition of KORC in the same protoplast by changing from 30 mM KCl in the bath to 30 mM TEA-Cl. Steps of 500-ms duration started from a holding potential of −30 mV and went to voltages between 70 and −10 mV, and between −40 and −100 mV, in decrements of 20 mV. C, Currents measured in the experiment shown in A and B, at 500 ms into each pulse, were plotted against voltage. ○, KCl in the bath; ●, TEA-Cl in the bath. Filter frequency, 100 Hz. Solutions: Pipette, 120 mM KCl, 0.15 µM free Ca^{2+}, 2 mM MgATP, 10 mM EGTA, and 10 mM Tris, pH 7.2; bath, 30 mM KCl or TEA-Cl, 1 mM $CaGlc_2$, 2 mM $MgCl_2$, and 10 mM MES, pH 5.8.

DISCUSSION

Diversity of the Anion Conductances

In our investigation, we suppressed all K^+ currents through the plasmalemma of the xylem parenchyma protoplasts by the use of TEA^+ or NMG^+ in the solutions, and therefore K^+ currents were not detected. Currents appearing in response to voltage ramps or sequences of voltage pulses were zero at the equilibrium potentials of Cl^- or $NO_3{}^-$; these were anion currents. The analysis of these electrical responses indicated the presence of three distinctly different anion conductances, which we called X-IRAC, X-QUAC, and X-SLAC (Table II; Fig. 11).

The X-IRAC appeared in 11% of the protoplasts if the Ca^{2+} concentration in the pipette was 0.15 µM, and in 34% if Ca^{2+} was 5 µM. It was characterized by open times of up to several seconds and was active in the voltage range from −180 to 50 mV (Fig. 1). This is most likely identical to the "slow" anion channel described by Wegner and Raschke

Table II. *Relative frequencies of activity of the three anion conductances in protoplasts prepared from the xylem parenchyma of roots of barley*

Percentage of protoplasts in which the respective conductance was active at a low and a high intracellular concentration of Ca^{2+}. Absolute numbers of protoplasts investigated are given in parentheses. The activities of X-IRAC and X-QUAC were significantly correlated with the internal Ca^{2+} concentration (χ^2-test, *, $P = 0.05$, **, $P = 0.005$). Determinations of X-QUAC and X-IRAC were made in external standard solution. Data on the activity of X-SLAC included measurements with external 1 and 40 mM Ca^{2+}. If data obtained solely with external standard solution were considered, X-SLAC was active in four out of 59 protoplasts, which again resulted in a percentage of 7.

Conductance Type	[Ca^{2+}] in the Pipette	
	0.15 μM	5 μM
	%	
X-IRAC	11** (9 out of 84)	34** (25 out of 74)
X-QUAC	27* (16 out of 59)	10* (7 out of 68)
X-SLAC	7 (7 out of 104)	0 (0 out of 68)

(1994), which had a mean open time of 1 s. The conductance X-IRAC is an inward rectifier. We showed in Figure 2 that this property could not have been the consequence of a concentration gradient, but must have resulted from intrinsic properties of the channel. The single-channel conductance of X-IRAC increased with hyperpolarization. At −130 mV, the chord conductance was 71 pS, and decreased to less than 13 pS near E_{Cl^-}. Without taking the rectifying effect into account, Wegner and Raschke (1994) estimated the conductance to be in the range of 46 to 85 pS at the same Cl^- concentrations we used; thus, the magnitudes of the conductances agreed with each other.

The channel X-IRAC shares features with an anion channel from amaranth cotyledons (Terry et al., 1991) and an anion channel in suspension cells derived from barley embryos (Amtmann et al., 1997). Both possessed slow gating characteristics and large conductances, and were selective for Cl^-. Similar to X-IRAC, the anion channel from barley embryos was strongly inward rectifying. It was active in the voltage range between −150 and 70 mV, and the open probability was only weakly voltage dependent (Amtmann et al., 1997). The anion channel from amaranth also activated at hyperpolarization (Terry et al., 1991). As also found in X-IRAC, activation was favored by a high intracellular Ca^{2+} concentration. A role of this channel was seen in the control of the membrane potential (Terry et al., 1991). Subconductance states are known to occur in anion channels in the plasma membrane of higher plants (Schauf and Wilson, 1987; Terry et al., 1991) and algae (Coleman, 1986; Laver, 1991). Figure 1 shows that, at hyperpolarization, subconductance states also occurred in X-IRAC.

Typical for X-QUAC was an activation within milliseconds (Fig. 5). Plasma membrane anion channels with similar characteristics occur in various plant species. Some of these channels activated rapidly with depolarization (Keller et al., 1989; Cerana and Colombo, 1992; Skerrett and Tyerman, 1994; Zimmermann et al., 1994; Thomine et al., 1995), others with hyperpolarization (Schauf and Wilson, 1987; Barbara et al., 1994; Elzenga and Van Volkenburgh, 1997).

The current-voltage curve of X-QUAC displayed a local maximum, followed, with increasing voltage, by a concavity (in Fig. 5, the maximum appeared at −40 mV and the minimum near 0 mV). This concavity resembles that of the current-voltage relationship of the rapidly activating anion channel of guard cells (Keller et al., 1989; Hedrich et al., 1990); however, currents through X-QUAC increased with hyperpolarization, whereas currents through the rapidly activating anion channel of guard cells declined. The inactivation of X-QUAC after voltage steps going to negative values (Fig. 5) is shared with other hyperpolarization-activated anion channels (Barbara et al., 1994; Elzenga and Van Volkenburgh, 1997).

One could consider the possibility that the two branches of the current-voltage relationship of X-QUAC (at negative and at positive voltages) were manifestations of two separate anion conductances, one inward rectifier and one outward rectifier. Indeed, tail currents recorded after returning from negative and from positive pulses to the holding voltage differed in their time courses. However, the anion-channel blocker DIDS (4,4′-diisothiocyanostilbene-2,2′-disulfonic acid) inhibited currents evoked by negative voltages as much as those produced by positive voltages (Köhler and Raschke, 1998a), and we never saw the sole activation of just one of the two branches. Alternatively, the conductance X-QUAC could have been only apparent, resulting from a summation of simultaneous activities of X-IRAC and X-SLAC; but the clearly distinct kinetics of X-QUAC and X-SLAC preclude this possibility (compare the current responses of these two conductances with the voltage pulses shown in Figs. 5A, 8A, and 9,A and B). We consider the one-conductance hypothesis of X-QUAC as the simplest explanation of our experimental results and are elaborating on it further at present (B. Köhler, L.H. Wegner, and K. Raschke, unpublished data).

The anion conductance with slow responses, X-SLAC, appeared in 7% out of a population of 104 protoplasts. Although its slow gating characteristics was reminiscent of those of X-IRAC, it differed from it in its voltage dependency. X-IRAC was active well below −100 mV (Figs. 1 and 2), whereas X-SLAC was active at voltages above −100 mV (Fig. 8). Deactivation of X-SLAC (Fig. 8A) was much slower than that of X-QUAC (Fig. 5A). After a voltage step, it took more than 30 s before a new steady state was established (Fig. 8). In this respect, there is some resemblance to the slowly activating anion channel of guard cells (Linder and Raschke, 1992; Schroeder and Keller, 1992), whose half-time of deactivation was 10 s after a voltage step from 20 to −120 mV (Schmidt and Schroeder, 1994). The slow anion conductance of guard cells was active over a wide voltage range, extending from below −200 to 50 mV and had a current minimum (corresponding to a maximum of anion efflux) near −40 mV (Linder and Raschke, 1992).

In three out of 23 experiments in which X-QUAC was active, a simultaneous activity of X-IRAC appeared, and three of our voltage-ramp experiments indicated a concurrent activity of X-QUAC and X-SLAC. The display of two types of anion conductance in one cell type was reported from guard cells of *Vicia faba* and *Xanthium strumarium* (Linder and Raschke, 1992; Schroeder and Keller, 1992) and

epidermal cells of the Arabidopsis hypocotyl (Thomine et al., 1995; Cho and Spalding, 1996). An apparent interconversion between quick and slow gating modes of an anion channel in guard cells of *V. faba* was reported by Dietrich and Hedrich (1994). Anion channels in tobacco suspension cells and epidermal cells of the Arabidopsis hypocotyl also appear to switch between quick and slow gating modes (Zimmermann et al., 1994; Thomine et al., 1995). It was suggested that these changes were caused by changes in the channel protein; this modulation depended on phosphorylation (Zimmermann et al., 1994) or the presence of ATP (Thomine et al., 1995).

Alternations between gating modes of anion channels also occur in animal cells, and are controlled by voltage, nucleotides, phosphorylation, or other, unknown factors (Fischer and Machen, 1994; Larsen et al., 1996). Although we have not yet obtained evidence for transitions between X-QUAC, X-SLAC, and X-IRAC in xylem parenchyma cells, we cannot exclude the possibility that just one protein accounts for the observed diversity, as an alternative to the activity of three different channel proteins. We also have to consider the fact that each xylem parenchyma cell disintegrated into an average of six protoplasts during the isolation procedure (Wegner and Raschke, 1994). If one protoplast of a preparation displayed only one type of anion conductance and a second protoplast another type, this could have been the result of an inhomogeneity in the distribution of conductances in the plasmalemma of the whole cell and a disconnection of the conductance ensemble during the division into subprotoplasts.

Control by Ca^{2+}

There was variability in the appearance of the three anion conductances. This should not be surprising, since ion transport from the root to the shoot is likely to be regulated and ion channels are conceivable effectors in this system, possibly with each type responding to a variety of signals. One presumed messenger is Ca^{2+}. Two of the conductances, X-QUAC and X-IRAC, responded to variations in "cytoplasmic" Ca^{2+} but, interestingly, in opposite ways. Whereas X-QUAC was active with 0.15 μM Ca^{2+} in the pipette and less so with 5 μM, the activity of X-IRAC grew larger with the same change. In this context it is worth noting that KORC is active at intracellular Ca^{2+} concentrations of 0.15 μM, and is inhibited by increasing Ca^{2+} levels (Wegner and De Boer, 1997); KORC therefore goes hand in hand with X-QUAC in regard to Ca^{2+} dependence. This parallel behavior supports the notion that X-QUAC and KORC provide the main pathways for electroneutral salt loading into the xylem.

The conductance X-SLAC was active at intracellular Ca^{2+} concentrations in the nanomolar range as well, and it might also be involved in xylem loading. In none of our experiments did the extracellular Ca^{2+} concentration appear to be a modulating factor. Variations of external Ca^{2+} in the range between 1 and 40 mM did not affect the anion conductances X-QUAC and X-IRAC (not shown), and Wegner et al. (1994) and Wegner and De Boer (1997) showed that the K^+ conductances KORC and KIRC were also insensitive to external Ca^{2+}. Ca^{2+} concentrations in xylem sap of various species range between 0.2 and 13 mM (Allen et al., 1988; Atkinson et al., 1992; Engels and Marschner, 1993; Schurr and Schulze, 1995; Zornoza et al., 1996).

Permeabilities for NO_3^- and Malate

NO_3^- is quantitatively the most important inorganic anion that is transported from the root through the xylem to the shoot. The permeability of X-IRAC for NO_3^- was equal to that for Cl^- (Fig. 4), and X-QUAC was three times more permeable for NO_3^- than for Cl^- (Table I). Thus, X-IRAC and X-QUAC may have a function in xylem loading with NO_3^-. Although we did not test the permeability of X-SLAC for NO_3^-, one can say that, in general, a high permeability for NO_3^- is a common feature of plant anion channels (Schönknecht et al., 1988; Keller et al., 1989; Terry et al., 1991; Tyerman, 1992; Hedrich and Marten, 1993; Schmidt and Schroeder, 1994; Skerrett and Tyerman, 1994). However, there is another side to the fact that the permeabilities for NO_3^- and Cl^- of the anion conductances in the barley root were of about equal magnitude. Apparently, there is little discrimination against Cl^-, and barley is known to be a salt includer (Wolf and Jeschke, 1986). It would be worth testing whether the anion conductances of roots of salt excluders (such as maize) possess a reduced permeability for Cl^-, relative to that for NO_3^-. Figure 7 indicates that NO_3^- may affect the electrical properties of X-QUAC. We have begun to explore this possibility.

Malate is thought to move in the plant from the shoot to the root at least in part through the phloem (Ben-Zioni et al., 1971; Kirkby and Knight, 1977), to be released into the apoplast of the root and ending up in the xylem sap. The permeability of X-QUAC for malate turned out to be smaller than that for NO_3^- or Cl^- (Table I), and the permeability sequence was similar to that of the quickly activating anion conductance of guard cells, NO_3^- (4.2) > Cl^- (1) > malate (0.1) (Hedrich and Marten, 1993). (In both investigations, it was the external malate that was changed.) Because the response to malate of the quickly activating anion channel of guard cells did not significantly change with a rise in pH from 5.6 to 7.2, malate^{2-} seemed to represent the active form of the metabolite (Hedrich and Marten, 1993). We assumed that it was also malate^{2-} that permeated X-QUAC at pH 5.8 in the external solution. At this pH, 83% of the malate is in the doubly charged form (pK_1 = 3.5; pK_2 = 5.1). There appeared to be some relationship with the quickly activating anion channel of guard cells, in which the current-voltage curve was modified by the presence of external malate. The activation potential and the concavity of the current-voltage relationship of the guard cell conductance moved to more hyperpolarized values with 82 mM malate (Hedrich and Marten, 1993). This was not the case with X-QUAC. Nevertheless, the decrease in anion efflux after the addition of external malate (Fig. 7A) is an indication that malate in the xylem sap might have a function in controlling X-QUAC, for instance by binding to an external site, as was reported to occur with the quickly activating anion channel of guard cells (Hedrich and Marten, 1993). Malate can provide neg-

ative charges in the xylem fluid, e.g. in NH_4^+-grown plants (Arnozis and Findenegg, 1986; Marschner, 1995). Further experiments should be directed at the question of whether malate modifies the properties of X-QUAC. If so, malate in the xylem sap could act as a messenger by controlling membrane potential in the xylem parenchyma and anion currents into the xylem vessels.

Estimation of Salt Fluxes into the Xylem

If salt release into the xylem is passive, two requirements must be met: the electrochemical potential gradients of the ions to be transported must be downhill into the xylem, and the voltage across the plasmalemma must be in a range at which anion and cation conductances are open simultaneously. Therefore, the equilibrium potentials of cations and anions set limits within which an electroneutral flux of anions and cations can occur. Under the conditions we assumed to apply, this was the case in the range from −30 to 30 mV (hatched area in Fig. 11). We also have to consider the limits set by the voltage dependencies of the ion conductances. An efflux of K^+ through KORC can occur only at voltages above −50 mV (Wegner and Raschke, 1994). All of the three anion conductances, X-IRAC, X-QUAC, and X-SLAC are active beyond this boundary (Fig. 11).

From the current-voltage relationships of the anion conductances we computed fluxes into the xylem (see "Materials and Methods"). Anion efflux through X-QUAC was larger than through X-IRAC or X-SLAC. Mean fluxes relative to fresh weight (in grams) were estimated to have been 11 μmol g^{-1} h^{-1} for X-QUAC, 8 μmol g^{-1} h^{-1} for X-SLAC, and 5 μmol g^{-1} h^{-1} for X-IRAC. These numbers exceed considerably the measured values of Pitman (1971, 1982) for the release of Cl^- from the xylem of barley roots; they ranged between 0.2 and 4 μmol g^{-1} h^{-1}. Anomalous mole-fraction effects were not considered here, but may have to be included in future estimations; we refer for instance to the work of Dietrich and Hedrich (1998) on the quickly activating anion channel of guard cells.

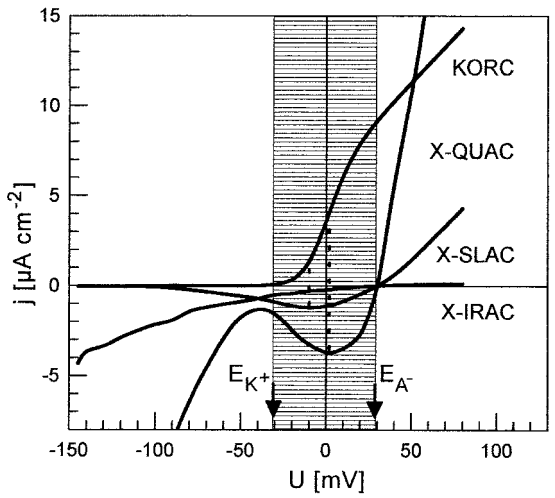

Figure 11. Representative current-voltage curves of the three anion conductances X-QUAC, X-SLAC, and X-IRAC juxtaposed to that of the KORC to recognize the voltage range in which anions and the cation K^+ could be released simultaneously into the xylem. The curve for X-IRAC depicts a series of products of *nP* by single-channel currents at the respective voltages. Data for KORC are from Wegner and Raschke (1994). Hatched area, Voltage range in which salt release appears possible; dotted lines, examples for simultaneous anion and K^+ currents of equal magnitude but opposite sign through X-SLAC and KORC in one case, and through X-QUAC and KORC in the other.

All three anion conductances may contribute to xylem loading (Fig. 11). However, we suggest that X-QUAC is the most important because of its large transport capacity and its activity at physiological Ca^{2+} concentrations (0.15 μM in our experiments). X-SLAC appeared less often and with smaller currents than through X-QUAC. Currents passing X-IRAC were very small in the range between the equilibrium potentials of K^+ and the major transported anions. We think it is possible that the main function of X-IRAC is not in facilitating salt release. Its single-channel conductance was largest at hyperpolarization, outside the range between the equilibrium potentials for K^+ and the major anions (Figs. 2, 4, and 11). It could provide a path for counter ions for H^+ during the activity of an electrogenic pump, which we found active in the plasmalemma of the xylem parenchyma cells (Köhler and Raschke, 1998b). The resulting acid secretion could have a function in a hypothetical regulation of pH in the xylem.

In conclusion, the finding of anion conductances of a transport capacity matching that of KORC in the cells of the xylem parenchyma in roots of barley reinforces the notion that the electroneutral loading of the xylem with K^+, NO_3^-, and Cl^- is a passive process.

ACKNOWLEDGMENTS

The authors thank L.H. Wegner for helpful comments on the manuscript, and M. Läsche, W.S. Peters, and B. Raufeisen for the great help they gave in the preparation of the figures.

Received May 10, 1999; accepted September 14, 1999.

LITERATURE CITED

Adam G, Läuger P, Stark G (1988) Physikalische Chemie und Biophysik, Ed 2. Springer-Verlag, Berlin

Allen S, Raven JA, Sprent JI (1988) The role of long-distance transport in intracellular pH regulation in *Phaseolus vulgaris* grown with ammonium or nitrate as nitrogen source, or nodulated. J Exp Bot **39:** 513–528

Amtmann A, Laurie S, Leigh R, Sanders D (1997) Multiple inward channels provide flexibility in Na^+/K^+ discrimination at the plasma membrane of barley suspension culture cells. J Exp Bot **48:** 481–497

Arnozis PA, Findenegg GR (1986) Electrical charge balance in the xylem sap of beet and *Sorghum* plants grown with either NO_3^- or NH_4^+ as inorganic nitrogen source. J Plant Physiol **125:** 441–449

Atkinson CJ, Ruiz LP, Mansfield TA (1992) Calcium in xylem sap and the regulation of its delivery to the shoot. J Exp Bot **43:** 1315–1324

Barbara JG, Stoeckel H, Takeda K (1994) Hyperpolarization-activated inward chloride current in protoplasts from suspension-cultured carrot cells. Protoplasma **180:** 136–144

Ben-Zioni A, Vaadia Y, Lips SH (1971) Nitrate uptake by roots as regulated by nitrate reduction products of the shoot. Physiol Plant **24:** 288–290

Caspary R (1865–1866) Bemerkungen über die Schutzscheide und die Bildung des Stammes und der Wurzel. Jahrbücher f wiss Botanik **4:** 101–124

Cerana R, Colombo R (1992) K^+ and Cl^- conductance of *Arabidopsis thaliana* plasma membrane at depolarized voltages. Bot Acta **105:** 273–277

Cho MH, Spalding EP (1996) An anion channel in *Arabidopsis* hypocotyls activated by blue light. Proc Natl Acad Sci USA **93:** 8134–8138

Clarkson DT (1993) Roots and the delivery of solutes to the xylem. Philos Trans R Soc Lond Ser B Biol Sci **341:** 5–17

Coleman HA (1986) Chloride currents in *Chara*: a patch-clamp study. J Membr Biol **93**: 55–61

Dietrich P, Hedrich R (1994) Interconversion of fast and slow gating modes of GCAC1, a guard cell anion channel. Planta **195:** 301–304

Dietrich P, Hedrich R (1998) Anions permeate and gate GCAC1, a voltage-dependent guard cell anion channel. Plant J **15:** 479–487

Elzenga JTM, Van Volkenburgh E (1997) Kinetics of Ca^{2+}- and ATP-dependent, voltage-controlled anion conductance in the plasma membrane of mesophyll cells of *Pisum sativum*. Planta **201:** 415–423

Engels C, Marschner H (1993) Influence of the form of nitrogen supply on root uptake and translocation of cations in the xylem exudate of maize (*Zea mays* L.). J Exp Bot **44:** 1695–1701

Fischer H, Machen TE (1994) CFTR displays voltage dependence and two gating modes during stimulation. J Gen Physiol **104:** 541–566

Führ KJ, Warhol W, Gratzl M (1993) Calculation and control of free divalent cations in solutions used for membrane fusion studies. Methods Enzymol **221:** 149–157

Gaymard F, Pilot G, Lacombe B, Bouchez D, Bruneau D, Boucherez J, Michaux-Ferrière NM, Thibaud JB, Sentenac H (1998) Identification and disruption of a plant Shaker-like outward channel involved in K^+ release into the xylem sap. Cell **94:** 647–655

Hamill O, Marty A, Neher E, Sakmann B, Sigworth F (1981) Improved patch-clamp techniques for high-resolution current recording from cells and cell-free membrane patches. Pflueg Arch Eur J Physiol **391:** 85–100

Hedrich R, Busch H, Raschke K (1990) Ca^{2+} and nucleotide dependent regulation of voltage dependent anion channels in the plasma membrane of guard cells. EMBO J **9:** 3889–3892

Hedrich R, Marten I (1993) Malate-induced feedback regulation of plasma membrane anion channels could provide a CO_2 sensor to guard cells. EMBO J **12:** 897–901

Hewitt EJ, Smith TA (1975) Plant Mineral Nutrition. English Universities Press, London

Hille B (1992) Ionic Channels of Excitable Membranes, Ed 2. Sinauer Associates, Sunderland, MA

Keller BU, Hedrich R, Raschke K (1989) Voltage-dependent anion channels in the plasma membrane of guard cells. Nature **341:** 450–453

Kirkby EA, Knight AH (1977) Influence of the level of nitrate nutrition on ion uptake and assimilation, and cation-anion balance in whole tomato plants. J Plant Physiol **60**: 349–353

Köhler B, Raschke K (1998a) X-QUAC, an anion conductance for loading nitrate into the xylem of barley roots. *In* Experimental Biology Online, Vol 3, Abstract, 11th International Workshop on Plant Membrane Biology, Cambridge, UK. Springer, Berlin. http://link.springer.de/link/service/journals/00898/toc.htm

Köhler B, Raschke K (1998b) An electrogenic pump in cells of the xylem parenchyma of barley roots. *In* Experimental Biology Online, Vol 3. Abstract, 11th International Workshop on Plant Membrane Biology, Cambridge, UK. Springer, Berlin. http://link.springer.de/link/service/journals/00898/toc.htm

Larsen EH, Gabriel SE, Stutts MJ, Fullton J, Price EM, Boucher RC (1996) Endogenous chloride channels of insect-Sf9 cells: evidence for coordinated activity of small elementary channel units. J Gen Physiol **107:** 1–20

Laver DR (1991) A surgical method for accessing the plasmamembrane of *Chara australis*. Protoplasma **161:** 79–84

Linder B, Raschke K (1992) A slow anion channel in guard cells, activating at large hyperpolarization, may be principal for stomatal closing. FEBS Lett **313:** 27–30

Marschner H (1995) Mineral Nutrition of Higher Plants, Ed 2. Academic Press, London

Marty A, Neher E (1995) Tight-seal whole-cell recording *In* B Sakmann, E Neher, eds, Single-Channel Recording, Ed 2. Plenum Press, New York

Neher E (1992) Correction for liquid junction potentials in patch-clamp experiments. Methods Enzymol **207:** 123–130

Pitman MG (1971) Uptake and transport of ions in barley seedlings. I. Estimation of chloride fluxes in cells of excised roots. Aust J Biol Sci **24:** 407–421

Pitman MG (1982) Transport across plant roots. Q Rev Biophys **15:** 481–554

Roberts SK, Tester M (1995) Inward and outward K^+-selective currents in the plasma membrane of protoplasts from maize root cortex and stele. Plant J **8:** 811–825

Schauf CL, Wilson KJ (1987) Properties of single K^+ and Cl^- channels in *Asclepias tuberosa* protoplasts. Plant Physiol **85:** 413–418

Schmidt C, Schroeder JI (1994) Anion selectivity of slow anion channels in the plasma membrane of guard cells. Plant Physiol **106:** 383–391

Schönknecht G, Hedrich R, Junge W, Raschke K (1988) A voltage dependent chloride channel in the photosynthetic membrane of a higher plant. Nature **336:** 589–592

Schroeder JI, Keller BU (1992) Two types of anion channel currents in guard cells with distinct voltage regulation. Proc Natl Acad Sci USA **89:** 5025–5029

Schurr U, Schulze ED (1995) The concentration of xylem sap constituents in root exudate, and in sap from intact, transpiring castor bean plants (*Ricinus communis* L.). Plant Cell Environ **18:** 409–420

Skerrett M, Tyerman D (1994) A channel that allows inwardly-directed fluxes of anions in protoplasts derived from wheat roots. Planta **192:** 295–305

Terry BR, Tyerman SD, Findlay GP (1991) Ion channels in the plasma membrane of *Amaranthus* protoplasts: one cation and one anion channel dominate the conductance. J Membr Biol **121:** 223–236

Tester M (1990) Plant ion channels: whole-cell and single channel studies. New Phytol **114:** 305–340

Thomine S, Zimmermann S, Guern J, Barbier-Brygoo H (1995) ATP-dependent regulation of an anion channel at the plasma membrane of protoplasts from epidermal cells of *Arabidopsis* hypocotyls. Plant Cell **7:** 2091–2100

Tyerman S (1992) Anion channels in plants. Annu Rev Plant Physiol Plant Mol Biol **43:** 351–373

Tyerman SD, Findlay GP (1989) Current-voltage curves of single Cl^--channels which coexist with two types of K^+-channels in the tonoplast of *Chara corallina*. J Exp Bot **40:** 105–117

Wegner LH, De Boer AH (1997) Properties of two outward-rectifying channels in root xylem parenchyma cells suggest a role in K^+ homeostasis and long-distance signalling. Plant Physiol **115:** 1707–1719

Wegner LH, De Boer AH, Raschke K (1994) Properties of the K^+ inward rectifier in the plasma membrane of xylem parenchyma cells from barley roots: effects of TEA^+, Ca^{2+}, Ba^{2+} and La^{3+}. J Membr Biol **142:** 363–379

Wegner LH, Raschke K (1994) Ion channels in the xylem parenchyma of barley roots: a procedure to isolate protoplasts from this tissue and a patch-clamp exploration of salt passageways into xylem vessels. Plant Physiol **105:** 799–813

Wolf O, Jeschke WD (1986) Sodium fluxes, xylem transport of sodium, and K/Na selectivity in roots of seedlings of *Hordeum vulgare*, cv. Villa. J Plant Physiol **125:** 243–256

Zimmermann S, Thomine S, Guern J, Barbier-Brygoo H (1994) An anion current at the plasma membrane of tobacco protoplasts shows ATP-dependent voltage regulation and is modulated by auxin. Plant J **6:** 707–716

Zornoza P, Gonzalez S, Serrano S, Carpena O (1996) Intervarietal differences in xylem exudate composition and growth under contrasting forms of N supply in cucumber. Plant and Soil **178:** 311–317